ADVANCED OPTICAL MATERIALS
www.advopticalmat.de

Light Phase Modulation with Transparent Paraffin-Based Phase Change Materials

Jaume R. Otaegui, Yannick Bertschy, Lorenzo Vallan, Falko Schmidt, Adarsh Vasista, Jose Garcia-Guirado, Claudio Roscini, Romain Quidant, and Jordi Hernando**

Phase change materials (PCM) have greatly contributed to optics with applications ranging from rewritable memories to smart windows. This is possible thanks to the variation in optical properties that PCMs undergo upon thermally-induced phase change. However, this behavior is accompanied by a loss of optical transparency in one (or more) of their phases, posing a major limitation for transmission-based functionalities. Here this challenge is addressed by producing PCM-based composites that remain transparent in the visible spectrum during their phase transition. The cornerstone of this innovative material is the use of 30 nm-in-size nanoparticles of paraffin as PCMs, which minimizes the scattering within the polymer host matrix regardless of the paraffin's phase. To demonstrate the potential of this approach, it is shown that thin composite layers can modulate the phase of the incident visible light using temperature, achieving uniform phase profiles with maximum phase shifts up to π radians. Notably, the composites studied exhibit up to threefold larger phase changes for the same input power over reference thermo-optical materials like polydimethylsiloxane. These findings position paraffin-based composites as promising materials for various thermo-optical applications, including wavefront shaping and aberration correction, with the potential to significantly impact a variety of optical technologies.

1. Introduction

Phase change materials (PCMs) are substances that undergo first-order phase transitions with temperature, such as melting processes, crystalline transformations, dehydration, or metallic-to-insulator transitions.[1,2] A large variety of PCMs exist and, depending on their nature can be classified as organic, inorganic, or eutectic mixtures.[3] The changes in their physical properties – e.g., thermal conductivity, refractive index (RI), or viscosity, along with the latent energy associated with their phase transitions make them attractive for a wide range of applications, including energy management,[4–7] solar light transmittance control,[8] thermochromic[9–12] and thermofluorochromic[13–18] materials, and drug delivery platforms,[19–22] among others.[23,24]

Of particular interest is the nonlinear behavior of the RI observed at temperatures near the phase transition of PCMs, a characteristic that can be harnessed for optical applications.[2,25–28] Historically, inorganic PCMs have often been the preferred choice due to their solid-to-solid state transitions, which exhibit a large contrast of both real (n) and imaginary (k) parts of the RI as well as fast switching speeds.[26,29] For example, germanium-antimony-tellurium (GST) and vanadium dioxide VO_2 are already employed commercially in optical data storage[26,30,31] and near-infrared filters,[32–35] respectively. Unfortunately, inorganic PCMs are typically expensive, scarce, difficult to process, and pose environmental concerns.[36,37] Additionally, they lack transparency in the visible region, which limits their suitability for transmission-based functionalities.[29,38] In contrast, organic PCMs such as paraffin and fatty alcohols have negligible k in the visible range, which could render them transparent across all phases despite the large change in RI (Δn) associated with their solid-liquid transition. Furthermore, their low cost and environmental friendliness make organic PCMs promising candidates for optical applications.[39–42]

To date, the use of organic PCMs in optics remains largely unexplored, with only a few reported instances of their incorporation into polymeric matrices.[8,42–45] These systems exploit the abrupt Δn associated with the PCM melting process to adjust the scattering intensity at the interface between the PCM

J. R. Otaegui, J. Hernando
Departament de Química
Universitat Autònoma de Barcelona
Edifici C/n, Campus UAB, Cerdanyola del Vallès 08193, Spain
E-mail: jordi.hernando@uab.cat

J. R. Otaegui, L. Vallan, C. Roscini
Catalan Institute of Nanoscience and Nanotechnology (ICN2)
CSIC and BIST
Campus UAB, Bellaterra, Barcelona 08193, Spain

Y. Bertschy, F. Schmidt, A. Vasista, J. Garcia-Guirado, R. Quidant
Nanophotonic Systems Laboratory
Department of Mechanical and Process Engineering
ETH Zurich, Zurich 8092, Switzerland
E-mail: rquidant@ethz.ch

The ORCID identification number(s) for the author(s) of this article can be found under https://doi.org/10.1002/adom.202401008

DOI: 10.1002/adom.202401008

and the polymer, due to the contrast in RI between the two components.[8,45] As a result, this change in scattering is accompanied by a corresponding shift in transparency, which has positioned PCM-polymer composites as promising, cost-effective, and scalable solutions for optical transmission filters that modulate the flux of light in response to temperature variations.[8,45] Furthermore, the availability of organic PCMs with a wide range of melting points (T_m) allows facile fine-tuning of the temperatures at which such light transparency modulation occurs.[8] Despite the advantages offered by organic PCM-polymer composites, their variable transparency poses a challenge for applications requiring high light transmittance. This is the case of light phase engineering, such as wavefront shaping or aberration correction, which is of relevance for optical imaging, free space optical communication, and integrated optical elements, amongst others.[47–51] Although there already exist technologies for light phase modulation such as Spatial Light Modulators (SLMs), they are expensive, polarization-dependent, and highly chromatic.[46] Alternatively, thermo-optical plates combine achromaticity across the entire visible range with high polarization insensitivity.[47–51] However, their reliance on homogeneous materials such as polydimethylsiloxane (PDMS) films, which exhibit moderate thermo-optical coefficients (dn/dT), requires high thermal heating to reach the desired RI modulation.[47–51] Unlocking the full potential of phase control for technological advancement therefore demands the development of novel materials that address these current limitations.

In this work, we introduce a set of PCM-polymer-based composites designed for light phase control which combine i) straightforward synthesis, affordability, and scalability; ii) high transparency in the visible wavelength spectrum (400–750 nm) independent of the PCM phase; and iii) higher thermo-optical coefficient in comparison to existing thermo-optical materials. These composites were produced by mixing paraffin nanoparticles (≈30 nm diameter) with a polymer matrix, enabling highly transparent films via simple drop-casting. Employing optical diffraction tomography, we measured a uniform phase response for such heterogeneously structured systems on the microscale. Finally, we benchmarked the composites against PDMS demonstrating that our materials not only outperform traditional thermo-optical plates in terms of energy efficiency but also exhibit comparable thermal properties and response times.

2. Results and Discussion

The speed at which light travels through a material is characterized by the material's RI and is influenced by several factors, including its density, internal structure, and composition. In thermo-optical materials, the RI varies with temperature, thus affecting the speed of light. Therefore, when a temperature gradient is generated within these media, a phase delay is introduced between light beams traversing through the material that are exposed to different temperatures, which can be exploited for wavefront modulation. Herein we hypothesize that temperature-dependent phase changes can be amplified with the use of organic PCMs, which typically undergo a density reduction during their solid-to-liquid transformation leading to a large decrease in RI and, consequently, a significant increase in the speed of light. However, to fully unleash the potential of organic PCMs' phase transition for thermo-optical applications, two important conditions must be met. First, PCMs must be integrated into a solid support that maintains its state regardless of temperature variation, thereby preserving the integrity of the system even after PCM melting. Second, the final composite material should possess high optical transparency across all wavelengths at the different phases of interest. To reach these goals, we propose embedding PCM nanoparticles (NPs) in a transparent polymer matrix that are sufficiently small to minimize light scattering irrespective of the PCM's phase. In these materials, the thermo-optical effect achieved should directly scale with the weight ratio of PCM NPs within the transparent composite film. Following this principle and through an appropriate choice of PCMs, the material's temperature profile could be precisely controlled, attaining on-demand modulation of the light's phase (**Figure 1**).

Amongst the various organic PCMs available, paraffins were selected due to their facile miniaturization and significant Δn upon solid-to-liquid transition (up to 0.07).[8] Moreover, paraffins are commercially available with varying alkyl lengths and, therefore, melting temperatures (T_m) at a low cost. Poly(vinyl alcohol) (PVA) was chosen as the polymer matrix in which PCM nanostructures were embedded due to several advantageous features: i) its ability to form uniform films[8,52] as well as excellent stabilizing properties for the preparation of nanoemulsions and paraffin particles' suspensions;[52,53] ii) its high transparency across the visible spectrum; iii) its comparable RI to solid state paraffins (n = 1.52 at room temperature); and iv) its low dn/dT value ($-1.9 \cdot 10^{-4}$ K^{-1}), ensuring that the overall thermo-optical performance of the paraffin-PVA composites is primarily determined by the embedded PCM (Figure S1, Supporting Information).

Based on this design, we synthesized various paraffin-PVA composites containing PCM NPs made of i) *n*-tetracosane (TC, T_m = 50.3 °C),[54] ii) *n*-eicosane (EC, T_m = 36.6 °C),[54] and iii) a 1:1 mixture of EC and *n*-octacosane (ECOC, T_m = 60.3 °C for OC).[54] All these NPs were prepared using a modified emulsion-entrapping technique,[53] where a heated aqueous solution of PVA (10 wt.%) was mixed with the melted paraffin and homogenized using an ultrasound tip to form PCM nanodroplets which, upon cooling, yielded the desired solid nanostructures. The obtained NPs showed an average diameter of ≈ 30 nm as measured by transmission electron microscopy (TEM), which is sufficiently small to reduce light scattering at the particle-polymer interface at optical wavelengths (**Figure 2**a,b for TC NPs; Figure S2, Supporting Information for EC and ECOC NPs). Uniform paraffin-PVA films of ≈ 175 µm in thickness (Figure 2c) and with a large content of PCM NPs (33 wt.%) were then obtained by drop-casting a mixture of the stabilized particles' suspension with aqueous PVA solution onto a plastic container (Figures S3 and S4, Supporting Information). Analysis of the cross-section of one of these films (TC-PVA) by scanning electron microscopy (SEM) showed that paraffin NPs were evenly dispersed within the polymer matrix despite the high payload, thus preventing nanoparticle aggregation or coalescence (Figure 2c, inset). This, together with the small size of the embedded NPs and the RI matching between PVA and the solid paraffin used, accounts for the high transparency exhibited by all composite films at room temperature regardless of the specific type of PCM (Figure 2d). The successful integration of PCM NPs into the PVA matrix was further demonstrated by differential scanning calorimetry (DSC), which revealed the

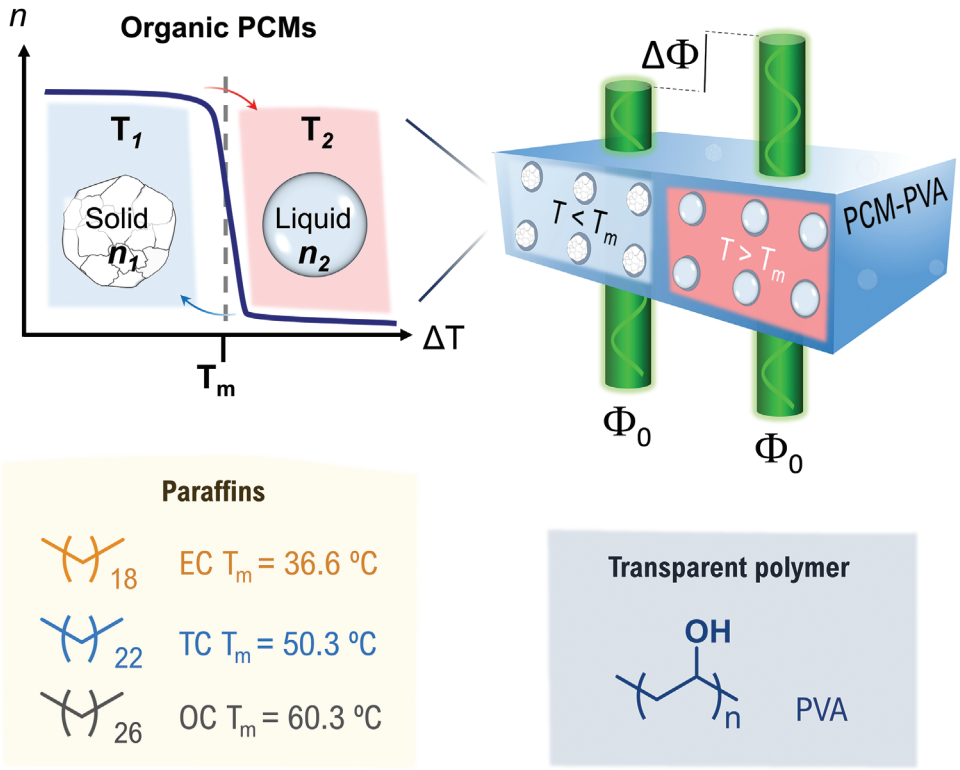

Figure 1. Conceptual scheme of the thermo-optical composite film based on organic PCMs. Paraffins of different melting points such as *n*-eicosane (EC), *n*-tetracosane (TC), or *n*-octacosane (OC) are embedded as NPs dispersed within a poly(vinyl alcohol) (PVA) polymer thin film. When exposed to heat, the paraffin NPs melt rapidly decreasing the overall RI of the composite layer due to the large d*n*/dT associated with the phase change of the PCM. As a result, if two light beams with the same input phase (Φ_0) travel through distinctly heated areas of the material where the paraffin NPs are in different states, the contrast in RI will induce a phase shift ($\Delta\Phi$).

occurrence of reversible phase transitions for the composite films at temperatures close to paraffins' bulk melting points (Figures S5 and S6, Supporting Information). Intriguingly, the TC-PVA composite exhibited an additional phase transition ≈ 40 °C in the DSC thermogram, an effect that has already been observed in other nanostructured paraffins and attributed to the triclinic to rotator transition (solid-to-solid phase transition),[55–59] which is not typically observed in bulk.[57,60] On the other hand, the broadened phase transition observed in ECOC-PVA film was associated with the merging of the phase transitions of the respective constituent PCMs.

The thermo-optical properties of all the fabricated paraffin-PVA film composites were subsequently investigated. First, temperature-controlled refractometry was used to monitor RI changes at λ = 558 nm when heated from 20 to 70 °C (**Figure 3a**, top). All measured films showed a decrease in RI of 0.04–0.05 within this thermal range: from 1.521 to 1.471 for TC-PVA, from 1.512 to 1.472 for EC-PVA, and from 1.513 to 1.479 for ECOC-PVA. However, the trend of the RI variation with temperature diverged significantly from each other. As expected, films containing pure paraffin NPs (TC-PVA and EC-PVA) showed a pronounced decrease in RI around the phase transition temperature of the corresponding bulk PCMs (T^{TC}_m = 50.3 °C[54] and T^{EC}_m = 36.6 °C)[54] –, i.e., when melting, which was accompanied by a more gradual RI reduction at other temperatures. Conversely, the ECOC-PVA film displayed a nearly linear RI change across the examined thermal range. This behavior can be attributed to different partially overlapping phase transitions of the two PCMs, resulting in the coexistence of distinct solid (triclinic and rotator) and liquid states and, thus, a more gradual RI shift, as previously corroborated by DSC analysis. Similar results were obtained when conducting temperature-dependent refractometry measurements at additional wavelengths in the visible spectrum (λ = 650, 589, 532, and 445 nm) (Figure S7, Supporting Information). As a result, the thermo-optical coefficients determined for the TC-PVA and EC-PVA films showed significant peak values around the melting temperature of the embedded PCMs ($dn/dT = -3.2{\cdot}10^{-3}$ K^{-1} at T = 56 °C and λ = 558 nm, and $-4.2{\cdot}10^{-3}$ K^{-1} at T = 41 °C and λ = 558 nm, respectively); by contrast, ECOC-PVA maintained a steadier dn/dT value of average $-0.8{\cdot}10^{-3}$ K^{-1} across the scanned temperature range (Figure 3a, middle). A strong correlation was observed between this thermo-optical behavior and the DSC thermograms measured for the paraffin-PVA layers, as illustrated by the nearly mirror-image equivalence between the dn/dT and thermal heating curves (see Figure 3a, bottom) – i.e., large RI variations coincide with paraffin phase transitions in the composite films. Consequently, this unambiguously validates that the thermo-optical properties of the PCM-PVA layers are governed by the thermal features of the embedded paraffin NPs, as originally devised.

Importantly, the large variation of RI determined for the paraffin-PVA composite films did not occur at the expense of

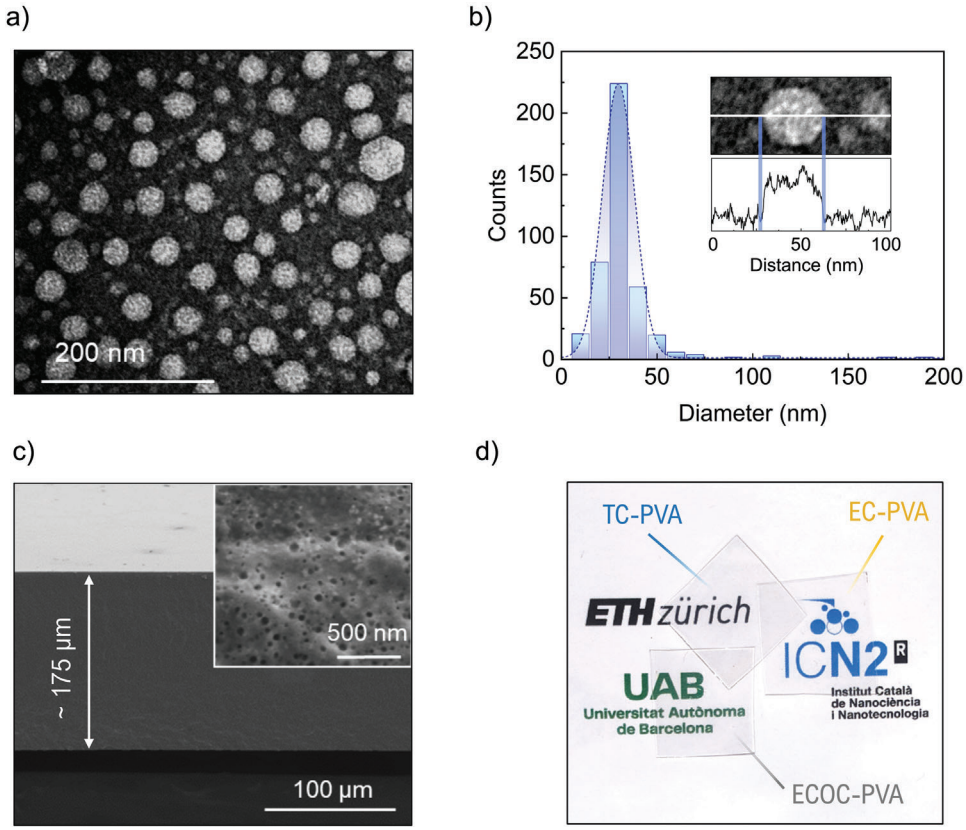

Figure 2. TC-PVA film characterization. a) TEM image of the TC NPs prepared. b) Histogram of the size of TC NPs showing an average particle size of 31 ± 11 nm. Inset: Measurement of the size of a single nanoparticle through the intensity value cross-section. c) SEM micrograph of the cross-section of a TC-PVA matrix film treated with chloroform to dissolve all remaining TC NPs on the outer surface. The inset shows the vacancies left on the surface after the PCM particles were extracted. d) Photograph of the different composite films prepared to demonstrate their high level of transparency (film thickness ≈175 µm). The logos were used with permission and according to our institutions' guidelines.

optical transparency, in contrast to previous reports for similar PCM-based composite layers.[8,44] As shown in Figure 3b, high visible light transmittance (*Tr*) was measured for all these materials across their operational temperature range – i.e., even after the melting of the embedded PCM NPs, when RI mismatching occurs between the liquid paraffin NPs (RI = 1.48–1.47 at λ = 589 nm) and the surrounding PVA matrix (RI = 1.52 at λ = 589 nm). Specifically, transmittance values between 80% and 88% were measured between 400 and 750 nm for all materials with the transmittance profiles remaining nearly invariant with temperature within the 500–750 nm spectral window. These results can be attributed to the minimal light scattering occurring within the composite films due to the small diameter of the dispersed PCM NPs (≈ 30 nm), which only slightly affects optical transparency at shorter wavelengths (400–500 nm) and at higher temperatures where paraffin particles melt and drastically vary their RI. This behavior was further proven by directly monitoring visible light scattering in the films by additional haze measurements (Figure S8, Supporting Information). Very low haze values that are consistent with high light transparency were obtained in all cases (<2.5%), which slightly increased upon paraffin melting due to the concomitant RI variation.

Following the optical characterization of the PCM-PVA films, we investigated their properties at the microscale, specifically, for regions of a few tens of microns in length, given the relevance of such scales for modern integrated optics. To do so, we employed an optical diffraction tomography (ODT) setup[61] to map the RI distribution near a microscopic heat source (**Figure** 4a). This interferometric technique captures the accumulated phase delay experienced by a probe laser beam as it traverses the sample at varying angles, enabling the reconstruction of the RI profile within a 50 × 50 × 20 µm^3 (≈50 pL) volume. A layer of uniformly distributed gold nanorods (AuNRs) deposited on a transparent substrate serves as a microscopic heat source when excited by a resonant-focused pump laser beam (Figure S9, Supporting Information).[62] The PCM-PVA sample, placed in direct contact with the AuNRs, experiences an RI gradient as the heat absorbed by the AuNRs diffuses into the material. Furthermore, by utilizing the experimental RI-to-temperature dependence (Figure 3a), we can evaluate the volumetric temperature distribution across the sample (Figure 4b).

For the ODT experiments, each PCM-PVA film was affixed to a glass substrate coated with AuNRs. A NIR laser (λ_{pump} = 808 nm, 60 mW) was used to adjust the temperature, while another laser (λ_{probe} = 465 nm, 0.3–0.7 mW) probed the RI distribution simultaneously. The system was designed to maximize the photothermal effect caused by the pump laser, as the absorption of the AuNRs' substrate was fivefold higher at 808 nm than at 465 nm,

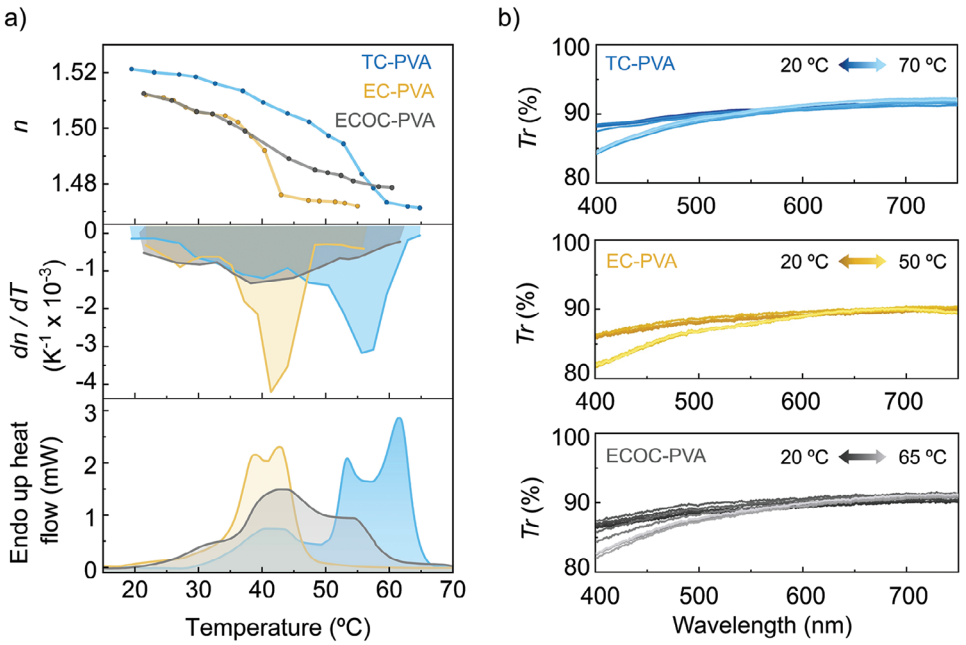

Figure 3. Thermo-optical properties of the PCM-PVA films. a) Comparison of the thermal dependence of RI ($\lambda = 589$ nm, top) and dn/dT (middle) with the DSC thermogram (down) for the three paraffin-PVA composite films: TC-PVA (blue), b) EC-PVA (yellow) and c) ECOC-PVA (grey). b) Transmittance spectra at different temperatures within the operational thermal range for each composite film, from lower (darker color) to higher (lighter). From top to bottom, results are shown for TC-PVA, EC-PVA, and ECOC-PVA films.

and the NIR irradiation power used was ≈ 100-fold higher (Figure S9, Supporting Information). Our observations confirmed that the temperature increased to ≈ 50 °C at the source plane, which generated a concomitant RI reduction in the irradiated area (≈ 1 μm^2). In particular, RI reductions of $\Delta n = -0.0193$, -0.0195, and -0.0221 were measured in this area for TC-, EC-, and ECOC-PVA composites, respectively. When moving away from the illuminated spot, the temperature and RI variations induced progressively decrease until fully vanishing at distances ≈ 10–15 μm (Figure 4b). This is clearly illustrated by Figure 4c, which shows the RI gradient profiles measured at various planes parallel to the heat source. Despite the films' heterogeneous nature and the different thermal conductivities of the PVA matrix and the paraffin nanostructures, a smooth and gradual RI variation was noted across the microscopic volume surrounding the irradiated area. We attribute this behavior to two main factors: the scale of observation of our ODT experiments (≈ μm), which is significantly larger than the NPs size (≈ 30 nm), and the isotropic distribution of paraffin NPs within the film, as shown in Figure 2c.

Adjusting the irradiation NIR power allowed for investigating the films under different temperature conditions. Figure 4d showcases the profiles of accumulated phase delay at 465 nm, or optical path difference (OPD), oriented perpendicularly to the source plane under varying irradiation levels. Notably, the OPD can be precisely adjusted by modulating the source temperature. Gradients up to π radians were achieved for all composites at temperatures ≈ 52, 42, and 42 °C, depending on the film's composition. These values of phase delay are in agreement with the local RI variations (up to −0.02) achieved within the small region of the composite films (≈ 10 μm in height) that is affected by photothermally heating in our experiments. In addition, OPD measurements remained consistent across different irradiation powers, underscoring the stability of the paraffin NPs within the films. When a pristine PVA film was examined, very small RI variations were observed under irradiation levels comparable to those used for the PCM composites (Figure S10, Supporting Information), indicating that the temperature-induced optical response is provided by the paraffin nanoparticles embedded in the film. The composites exhibited a significant thermo-optical effect, with a contrast of up to 4.5 folds at the central peak position in comparison to the pristine PVA film.

These results demonstrate that PCM-PVA composites can sustain spatially homogeneous gradients of RI, thereby facilitating phase modulation of light in thin films. To date, a limited selection of thermo-optical materials transparent within the visible spectrum has been investigated for light-phase engineering, including water, liquid glycerol, and PDMS.[47,49,51] Given their physical similarities and sample production requirements, we chose PDMS as a benchmark material against the PCM-PVA composites. In contrast, water and glycerol were less suitable due to their liquid state, which complicates their manipulation. PDMS possesses exceptional optical transparency, notable dn/dT for homogeneous polymers ($-3.4\ 10^{-4}$ K^{-1}), non-toxicity, and ease-of-use characteristics. PDMS films, matching the composites in thickness, were produced and positioned atop the AuNR-coated substrate, employing a methodology akin to that used for the composites. Subsequently, we characterized the local heat distribution and modulation speed and evaluated the power-to-phase magnitude relationship.

First, we employed ODT experiments to compare the performance of PCM-PVA and PDMS films in terms of heat diffusion upon local heating. This is a parameter of significant relevance in

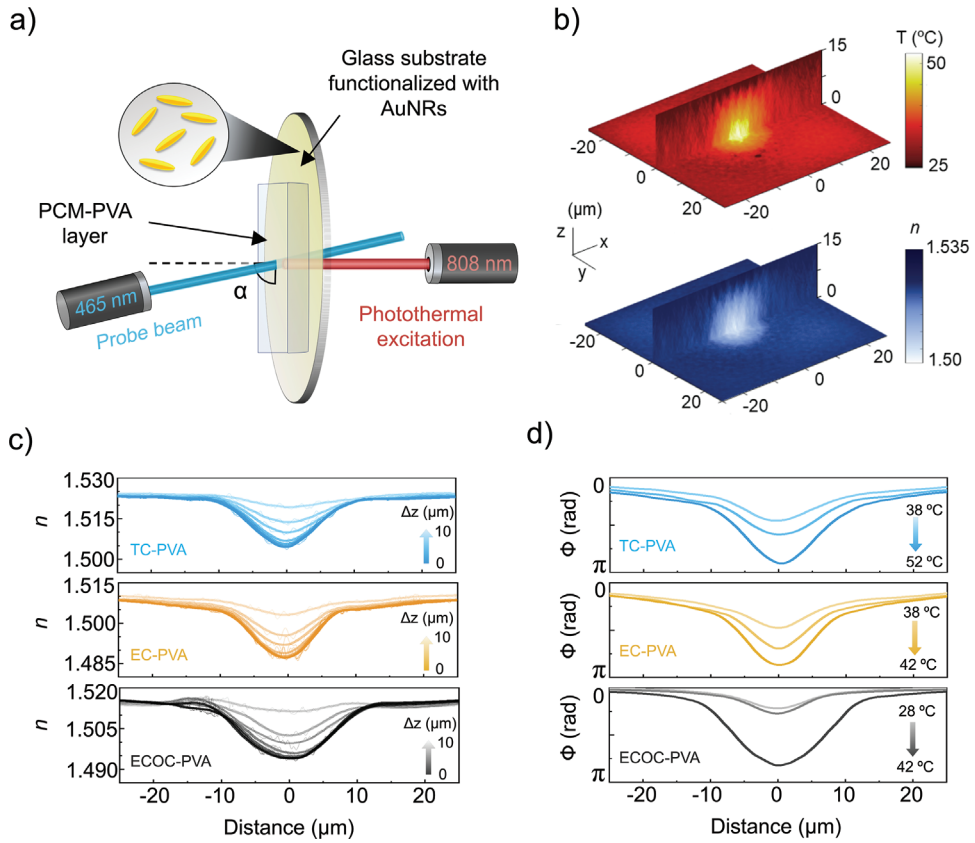

Figure 4. Microscale film's thermo-optical properties. a) Scheme of the sample configuration for the ODT measurements. The PCM-PVA composite film (PCM-PVA layer) was placed on top of a glass substrate functionalized with gold nanorods (AuNRs). When the substrate was irradiated at the resonant wavelength of 808 nm, the gold nanorods absorbed the incident light and converted it into heat creating a temperature gradient and, subsequently, a RI gradient in the composite, which were probed at 465 nm. b) Volumetric data retrieved from ODT measurements. 2D cross-sections (x-y and x-z) for the temperature (top) and the RI (bottom) of a TC-PVA film obtained through NIR light irradiation (power ≈ 60 mW). c) RI linear crosscuts of the x-y cross-section at increasing distances (at 0, 1, 2, 3, 5, 7 and 10 μm) from the heat source plane for the three PCM-PVA composites ($\lambda = 465$ nm). d) OPD linear crosscuts of the x-y cross-section obtained at increasing temperatures for the three PCM-PVA composites ($\lambda = 465$ nm).

microsystems, where multiple heated components could be positioned in close proximity to each other, thus potentially affecting their operation; therefore, precise spatial temperature control would be required in this case. With this aim, the PDMS and PCM-PVA films were subjected to local NIR irradiation at constant power to maintain a temperature of ≈ 50 °C, consistent with prior experiments. **Figure** 5a illustrates the cross-section of the temperature map for both the PDMS and the PCM-PVA layers at the heat source plane, with plots normalized to the maximum temperature for comparison. Despite minor variations, temperature confinement appeared uniform across all films. However, profile discrepancies emerge due to variations in thermal conductivity during the PCM phase transitions, which decrease from solid to liquid.[63] In particular, slightly narrower responses were measured for the composites in comparison to PDMS, suggesting tighter confinement of temperature changes in PCM-based materials.

Next, we investigated the films' phase time response upon local heating. Owing to a mismatch between the ODT setup's acquisition rates and the films' responses, a series of pump-probe measurement cycles, interspaced with cooldown periods, were conducted to ascertain the temperature dynamics with high temporal precision (200 μs), depicted in Figure 4b. The NIR irradiation power remained fixed with induced temperatures ≈ 50 °C. The phase delay for each measurement point was assessed, and then the responses of the various films were normalized to facilitate comparison. Notably, TC-PVA and PDMS films exhibited similar responses in the millisecond range (≈ 15 ms). In contrast, EC-PVA and ECOC-PVA films demonstrated slower reactions (Figure 5b), which can be attributed to the PCMs' physical state under experimental conditions. The latent heat necessary for the solid-to-liquid phase transition decelerated the response of EC- and ECOC-PVA films. Conversely, the TC-PVA film, poised near the phase transition temperature, closely matched the PDMS response with minimal discrepancy.

From an energy perspective, we assessed the induced phase modulations relative to the power required to generate heat in our setup. As in Figure 4d, the accumulated phase delay difference between the center of the heat source and the boundary values of the examined volume served as a metric for comparison across different laser powers. Figure 5c displays the modulation of composite films and PDMS under increasing laser power. Given the diverse phase transition temperatures and experimental setup constraints, film measurements were limited to phase

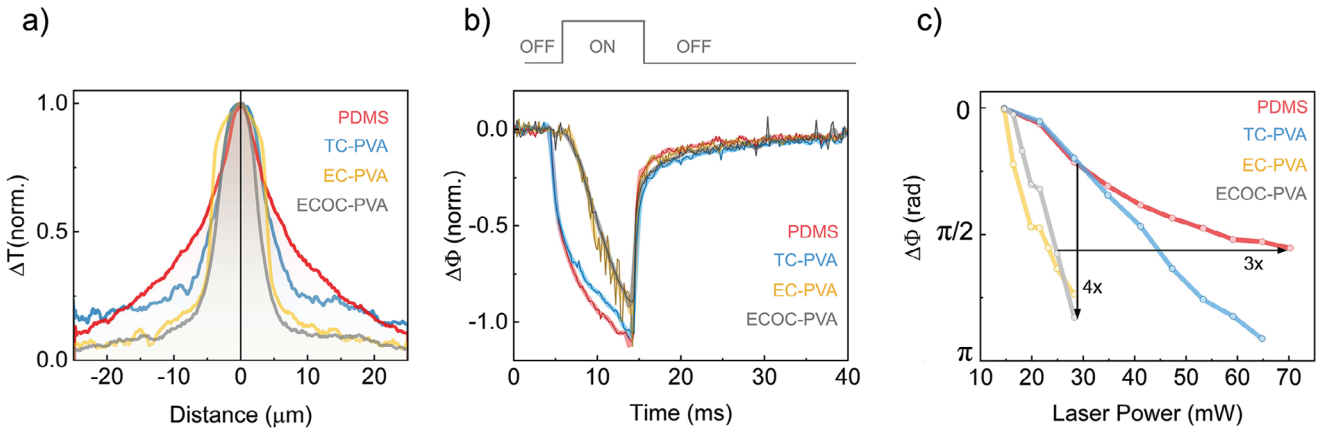

Figure 5. Benchmarking between the PCM-PVA and PDMS films revealed that the composites yielded a greater phase shift per unit of power injected, while simultaneously preserving speed and temperature confinement. a) Normalized temperature gradient crosscuts at the source plane. b) Normalized phase time response obtained by the pump-probe setup. c) Maximum phase difference versus source power. Color code: PDMS (red), TC-PVA (blue), EC-PVA (yellow), ECOC-PVA (gray).

gradients below π radians. As anticipated, the PCM-PVA composites exhibited greater modulations at lower power, resulting in decreased temperatures and, consequently, reduced operational energy. For instance, phase shifts close to π radians necessitated only 65, 28, and 28 mW for TC-, EC-, and ECOC-PVA, respectively, whereas PDMS required >70 mW. This is a remarkable result, as the phase transition enthalpy of PCMs necessitates an additional heat input absent in PDMS films. However, the greater magnitude of dn/dT associated with paraffin NPs' phase change sufficiently compensates for this requirement, enabling PCM-PVA-based films to generate phase gradients up to 4-fold larger than PDMS layers at equivalent irradiation powers.

3. Conclusion

In summary, we have experimentally validated the use of transparent composite polymer films based on phase change materials as viable thermo-optical media for modulating the phase of light. For this, we introduce herein a synthesis technique capable of creating thermo-optical materials made of paraffin nanoparticles embedded into non- or low-thermo-optical matrices. The operational range of these composites can be customized by selecting paraffins with the desired phase transition temperatures. Furthermore, their optical properties, time response, and energy consumption can be predicted simply from the transition temperature analyses. Our synthesis parameters facilitate the production of transparent films, of ≈ 175 μm in thickness, whose visible light transmittance remains effectively high (T_r >80%) across the entire temperature working range of the materials (25–55 °C) –, i.e., regardless of the state (solid or liquid) of the PCM. This optical feature was previously unachievable with reported PCM materials. A significant benefit of these new composites is their ability to yield higher phase shifts (up to four times), at reduced power levels in comparison to conventional PDMS-based thermo-optical materials. Moreover, the composite films maintain uniform properties at the micrometer scale and are versatile, supporting conformal coating beyond flat substrates. Crucially, the composites we propose are cost-effective, readily available, scalable, and comprised of non-toxic materials. They also offer simplicity in processing and can be effortlessly integrated with optical substrates. For these reasons, we anticipate that this material family will provide significant advantages to the optics community in the forthcoming years.

4. Experimental Section

Materials: All the phase change materials used (*n*-eicosane 99%, *n*-tetracosane 99%, *n*-octacosane 99%) were purchased from Alfa Aesar. Poly(vinyl alcohol) Mowiol PVA 4–88 (M_w = 31.000, hydrolysis 88%) and ethylene glycol (99.8%) were obtained from Sigma Aldrich. Poly(dimethylsiloxane) was produced using SYLGARD 184 from Dow Corning. All these chemicals were utilized without further purification.

Preparation of PCM NPs: First, 1 g of the desired paraffin (or a mixture of paraffins) was added into a 30 mL scintillation vial and mixed with 20 mL of a freshly prepared 10 wt.% aqueous solution of low molecular weight PVA (Mowiol PVA 4–88), previously heated at 60 °C under gentle stirring. When the paraffin was melted, the mixture was stirred for 1 h at 1000 rpm. After this pre-emulsification process, the mixture was transferred to a 50 mL beaker and placed in a hot water bath (≈ 60 °C). The sonication tip was submerged in the mixture (2/3 deep) and the mixture was sonicated for 5 min (10 s on and 10 s off) at 100% amplitude. This process was repeated 4 times (20 min of sonication in total). The volume of the emulsion was checked after every cycle and water was added to compensate for the liquid evaporated during the sonication process. Then, the sonicated emulsion was transferred to a scintillation vial and was left to cool down at room temperature under gentle stirring.

Preparation of PCM-PVA and PDMS Films: Typically, 4 g of the desired PCM NPs suspension (0.05 g mL^{-1}) in an aqueous solution of PVA (0.1 g mL^{-1}) was poured into a 5.5 cm in diameter polystyrene Petry dish, and the water solvent was let to evaporate under ambient conditions for 72 h. Afterward, a free-standing film with a 33 wt. % of embedded PCM NPs was obtained by easily peeling it off from the container. PDMS films were made using the standard 1:10 mixture ratio. Similarly to PVA films, liquid PDMS was poured on a hydrophobic silicon wafer in a petri dish and then baked for 1 h at 80 °C in a convection oven.

Characterization Methods: The morphology of PCM NPs was analyzed by transmittance electron microscopy (TEM) using a JEM-1400 (120 kV) microscope. The samples were prepared by drop-casting diluted suspensions of the NPs over carbon supported onto copper grids and stained with uranyl acetate (2 wt.%, 8 μL). The morphology of the obtained PCM-PVA films was analyzed by scanning electron microscopy (SEM) by means of an FEI Quanta 650 ESEM microscope applying a 5 kV voltage. The

samples were metalized with a platinum layer of ≈5 nm prior to SEM analysis. For the imaging of the crosscut section, the samples were not metalized The obtained films' RI was measured with an Atago Abbe NAR-1T SOLID refractometer, and the temperature of the sample was controlled with a heating/cooling recirculating bath (Huber MPC-K6). A calibration with mixtures of ethylene glycol (99.8%) and water was performed for the measurements of RI at wavelengths different from 589 nm.[64] Because of the high light transmittance of the samples at all the conditions investigated, no significant variation in precision was observed during the RI readings on the refractometer at different wavelengths and temperatures. The optical transmittance of PCM-PVA composites within the visible range was acquired by means of an Agilent Cary 60 spectrophotometer in transmission mode, while haze measurements were performed using a BYK-Gardner Haze-Gard i (4775) haze meter with a measurement area of 18 mm illuminated with CIE D65 LED. The temperature of the films was controlled using a custom-made holder (Sapphire 360, ES Patent ES1263094U) in which the films were kept between two sapphire windows attached to two copper sheets, which were connected to a temperature controller. DSC measurements were obtained using a TA instrument Q20. A temperature ramp rate of 10 °C min^{-1} was used for all the samples.

Sample Preparation for ODT Experiment: To perform the ODT measurements, the thermo-optical films of interest were attached to an Au nanorods-functionalized glass substrate. The gold nanorods were prepared using a method described by Nikoobakht et. al.[65] and the functionalization was achieved using a standard functionalization protocol.[62] To attach the films to the functionalized substrate, different procedures were followed depending on whether the film was made from PVA or PDMS. For the PVA-based films, the surface of the glass substrate was humidified with 2 µL of MilliQ water (Merk Direct-Q 3UV), and a piece (5 mm × 5 mm) of the PCM-PVA composite of interest or PVA film was stuck to the Au nanorods-glass surface. The assembled film was dried overnight in a vacuum chamber. For the PDMS sample, SYLGARD 184 was used. The film was cast with a similar method to the PCM-PVA films. The attachment to the AuNR substrate was made using an uncasted drop of PDMS between the film and the Au nanorods-glass substrate. Then, the sample was placed under vacuum for 2 h to degas, and finally, baked in the oven for 1 h at 80 °C to complete the cross-linking.

Optical Diffraction Tomography Measurements: Optical diffraction tomography (ODT) measurements were acquired utilizing the optical setup previously reported by us.[61] Briefly, a 465 nm probe laser (0.3–0.7 mW) was bifurcated into reference, and object beams with a fiber splitter, while illumination angles were modulated by rotating a wedge prism. Interferograms resulted from these beams interfering with a camera. camera. Optimized gold nanorods (80 NR $µm^{-2}$) for NIR absorption (Figure S9, Supporting Information) were excited with an 808 nm pump beam (60 mW) via a 40x objective lens, directing a non-expanded beam through a long focal lens to achieve a ≈10 µm spot size. An FPGA card synchronized the pump and probe lasers with camera acquisitions set at 10 Hz, adjusting pulse durations to experimental needs.

Supporting Information

Supporting Information is available from the Wiley Online Library or from the author.

Acknowledgements

The authors acknowledge the funding from MCIU/AEI/10.13039/501100011033 and ERDF – "A way of making Europe" through grants PID2021-127983OB-C21 and PDC2022-133368-I00, from Generalitat de Catalunya (AGAUR) through projects 2021 PROD 00190 and 2021 SGR 00064), and from the Swiss National Science Foundation (SNSF) through grant PROFIT (205936). The ICN2 is supported by the Severo Ochoa Centers of Excellence program, Grant CEX2021-001214-S, funded by MICIU/AEI/10.13039.501100011033. J.R.O. thanks the Generalitat de Catalunya (AGAUR) for his predoctoral FI fellowship.

Conflict of Interest

The authors declare no conflict of interest.

Data Availability Statement

The data that support the findings of this study are openly available in the repository CORA.RDR at https://dataverse.csuc.cat.

Keywords

light phase modulation, optical diffraction tomography, phase change materials, polymer composites, thermo-optical materials

Received: April 12, 2024
Revised: June 7, 2024
Published online: July 4, 2024

[1] D. C. Hyun, N. S. Levinson, U. Jeong, Y. Xia, *Angew. Chem., Int. Ed.* **2014**, *53*, 3780.
[2] J. Wang, L. Wang, J. Liu, *IEEE Access.* **2020**, *8*, 121211.
[3] M. Zare, K. S. Mikkonen, *Adv. Funct. Mater.* **2023**, *33*, 2213455.
[4] R. Guo, L. Shan, Y. Wu, Y. Cai, R. Huang, H. Ma, K. Tang, K. Liu, *Mater. Today Energy.* **2022**, *23*, 100888.
[5] T. Ma, H. Yang, Y. Zhang, L. Lu, X. Wang, *Renew. Sustain. Energy Rev.* **2015**, *43*, 1273.
[6] C. Alkan, A. Sarı, A. Karaipekli, *Energy Convers. Manag.* **2011**, *52*, 687.
[7] G. G. D. Han, J. H. Deru, E. N. Cho, J. C. Grossman, *Chem. Commun.* **2018**, *54*, 10722.
[8] J. R. Otaegui, D. Ruiz-Molina, J. Hernando, C. Roscini, *Chem. Eng. J.* **2023**, *463*, 142390.
[9] M. A. White, M. LeBlanc, *J. Chem. Educ.* **1999**, *76*, 1201.
[10] A. Yuan, S. Zhao, T. Liu, Y. Zhao, L. Jiang, J. Lei, *Adv. Mater. Technol.* **2022**, *7*, 2200226.
[11] Y. Zhang, H. Liu, J. Niu, X. Wang, D. Wu, *Appl. Energy.* **2020**, *264*, 114729.
[12] S. Liu, Y. Li, Y. Wang, K. M. Yu, B. Huang, C. Y. Tso, *Adv. Sci.* **2022**, *9*, 2106090.
[13] C. Bellacanzone, J. R. Otaegui, J. Hernando, D. Ruiz-Molina, C. Roscini, *Adv. Opt. Mater.* **2022**, *10*, 2102423.
[14] J. R. Otaegui, A. Carrascull-Marín, D. Ruiz-Molina, J. Hernando, C. Roscini, *Adv. Opt. Mater.* **2022**, *10*, 2200083.
[15] J. Du, L. Sheng, Y. Xu, Q. Chen, C. Gu, M. Li, S. X.-A. Zhang, *Adv. Mater.* **2021**, *33*, 2008055.
[16] K. Zhang, X. Zhou, S. Li, L. Zhao, W. Hu, A. Cai, Y. Zeng, Q. Wang, M. Wu, G. Li, J. Liu, H. Ji, Y. Qin, L. Wu, *Adv. Mater.* **2023**, *35*, 2305472.
[17] Y.-J. Jin, Y.-G. Choi, H. Park, G. Kwak, *J. Mol. Liq.* **2018**, *265*, 260.
[18] J. R. Otaegui, P. Rubirola, D. Ruiz-Molina, J. Hernando, C. Roscini, *Adv. Opt. Mater.* **2020**, *8*, 2001063.
[19] S.-W. Choi, Y. Zhang, Y. Xia, *Angew. Chem., Int. Ed.* **2010**, *49*, 7904.
[20] J. Qiu, D. Huo, Y. Xia, *Adv. Mater.* **2020**, *32*, 2000660.
[21] Y. Dai, J. Su, K. Wu, W. Ma, B. Wang, M. Li, P. Sun, Q. Shen, Q. Wang, Q. Fan, *ACS Appl. Mater. Interfaces.* **2019**, *11*, 10540.
[22] Q. Zhang, J. Liu, K. Yuan, Z. Zhang, X. Zhang, X. Fang, *Nanotechnology.* **2017**, *28*, 405101.
[23] N. Sarier, E. Onder, *Thermochim. Acta.* **2012**, *540*, 7.
[24] Y. Tan, X. Du, Z. Du, H. Wang, X. Cheng, *RSC Adv.* **2021**, *11*, 5712.
[25] M. S. Nisar, X. Yang, L. Lu, J. Chen, L. Zhou, *Photonics.* **2021**, *8*, 205.
[26] M. Wuttig, H. Bhaskaran, T. Taubner, *Nat. Photonics.* **2017**, *11*, 465.
[27] C. Ríos, L. Zhou, A.-K. U. Michel, A. Majumdar, J. Hu, *Opt. Mater. Express.* **2022**, *12*, 4284.

[28] X. Wang, H. Qi, X. Hu, Z. Yu, S. sss, Z. Du, Q. Gong, *Molecules*. **2021**, *26*, 2813.
[29] Y. Zhang, J. B. Chou, J. Li, H. Li, Q. Du, A. Yadav, S. Zhou, M. Y. Shalaginov, Z. Fang, H. Zhong, C. Roberts, P. Robinson, B. Bohlin, C. Ríos, H. Lin, M. Kang, T. Gu, J. Warner, V. Liberman, K. Richardson, J. Hu, *Nat. Commun.* **2019**, *10*, 4279.
[30] P. Guo, A. M. Sarangan, I. Agha, *Appl. Sci.* **2019**, *9*, 530.
[31] T. Cao, R. Wang, R. E. Simpson, G. Li, *Prog. Quantum Electron.* **2020**, *74*, 100299.
[32] X. P. Zhao, S. A. Mofid, T. Gao, G. Tan, B. P. Jelle, X. B. Yin, R. G. Yang, *Mater. Today Phys.* **2020**, *13*, 100205.
[33] P. Hu, P. Hu, T. D. Vu, M. Li, S. Wang, Y. Ke, X. Zeng, L. Mai, Y. Long, *Chem. Rev.* **2023**, *123*, 4353.
[34] X. Li, C. Cao, C. Liu, W. He, K. Wu, Y. Wang, B. Xu, Z. Tian, E. Song, J. Cui, G. Huang, C. Zheng, Z. Di, X. Cao, Y. Mei, *Nat. Commun.* **2022**, *13*, 7819.
[35] Y. Ke, C. Zhou, Y. Zhou, S. Wang, S. H. Chan, Y. Long, *Adv. Funct. Mater.* **2018**, *28*, 1800113.
[36] O. Okogeri, V. N. Stathopoulos, *Int. J. Thermofluids.* **2021**, *10*, 100081.
[37] S. A. Mohamed, F. A. Al-Sulaiman, N. I. Ibrahim, M.d. H. Zahir, A. Al-Ahmed, R. Saidur, B. S. Yılbaş, A. Z. Sahin, *Renew. Sustain. Energy Rev.* **2017**, *70*, 1072.
[38] S. S. Chandel, T. Agarwal, *Renew. Sustain. Energy Rev.* **2017**, *67*, 581.
[39] J. Yang, Y.-C. Zhou, L.-Y. Yang, C.-P. Feng, L. Bai, M.-B. Yang, W. Yang, *Adv. Funct. Mater.* **2022**, *32*, 2200792.
[40] R. K. Sharma, P. Ganesan, V. V. Tyagi, H. S. C. Metselaar, S. C. Sandaran, *Energy Convers. Manag.* **2015**, *95*, 193.
[41] M. M. Kenisarin, *Sol. Energy.* **2014**, *107*, 553.
[42] R. Yoshikawa, M. Tenjimbayashi, S. Shiratori, *ACS Appl. Energy Mater.* **2018**, *1*, 1429.
[43] Z. Qiu, S. Wang, Y. Wang, J. Li, Z. Xiao, H. Wang, D. Liang, Y. Xie, *Compos. Sci. Technol.* **2020**, *200*, 108407.
[44] Y. Xie, F. Guan, Z. Li, Y. Meng, J. Cheng, L. Li, Q. Pei, *Macromol. Rapid Commun.* **2020**, *41*, 2000290.
[45] Y. Liu, J. Fan, R. Plamthottam, M. Gao, Z. Peng, Y. Meng, M. He, H. Wu, Y. Wang, T. Liu, C. Zhang, Q. Pei, *Chem. Mater.* **2021**, *33*, 7232.
[46] C. Maurer, A. Jesacher, S. Bernet, M. Ritsch-Marte, *Laser Photonics Rev.* **2011**, *5*, 81.
[47] P. Berto, L. Philippet, J. Osmond, C. F. Liu, A. Afridi, M. Montagut Marques, B. Molero Agudo, G. Tessier, R. Quidant, *Nat. Photonics.* **2019**, *13*, 649.
[48] A. Afridi, J. Canet-Ferrer, L. Philippet, J. Osmond, P. Berto, R. Quidant, *ACS Photonics.* **2018**, *5*, 4497.
[49] J. S. Donner, J. Morales-Dalmau, I. Alda, R. Marty, R. Quidant, *ACS Photonics.* **2015**, *2*, 355.
[50] A. Archetti, R.-J. Lin, N. Restori, F. Kiani, T. V. Tsoulos, G. Tagliabue, *Nanophotonics* **2022**, *11*, 3969.
[51] H. M. L. Robert, K. Holanová, Ł. Bujak, M. Vala, V. Henrichs, Z. Lánský, M. Piliarik, *Nat. Commun.* **2021**, *12*, 2921.
[52] J. R. Otaegui, D. Ruiz-Molina, L. Latterini, J. Hernando, C. Roscini, *Mater. Horiz.* **2021**, *8*, 3043.
[53] H. Torres-Pierna, D. Ruiz-Molina, C. Roscini, *Mater. Horiz.* **2020**, *7*, 2749.
[54] A. H. Johnstone, *CRC Handbook of Chemistry and Physics—69th Edition Editor in Chief R. C. Weast*, CRC Press Inc, Boca Raton, Florida **1991**, p. 2400.
[55] Y. Zhu, Y. Chi, S. Liang, X. Luo, K. Chen, C. Tian, J. Wang, L. Zhang, *Sol. Energy Mater. Sol. Cells.* **2018**, *176*, 212.
[56] F. Cao, B. Yang, *Appl. Energy.* **2014**, *113*, 1512.
[57] G. Abdeali, A. R. Bahramian, M. Abdollahi, *J. Energy Storage.* **2020**, *29*, 101299.
[58] N. Jung, M. Yun, S. Jeon, *J. Chem. Phys.* **2012**, *136*, 104903.
[59] J. M. Khodadadi, L. Fan, H. Babaei, *Renew. Sustain. Energy Rev.* **2013**, *24*, 418.
[60] S. Liang, Q. Li, Y. Zhu, K. Chen, C. Tian, J. Wang, R. Bai, *Energy.* **2015**, *93*, 1684.
[61] A. B. Vasista, B. Ciraulo, F. Schmidt, J. Ortega Arroyo, R. Quidant, *Sci. Adv.* **2024**, *10*, eadk5440.
[62] B. Ciraulo, J. Garcia-Guirado, I. de Miguel, J. Ortega Arroyo, R. Quidant, *Nat. Commun.* **2021**, *12*, 2001.
[63] F. P. Fleming, L. de Andrade Silva, G. dos S V Lima, I. Herzog, H. R. B. Orlande, J.-L. Daridon, J. Pauly, L. F. A. Azevedo, *Fluid Phase Equilib.* **2018**, *477*, 78.
[64] V. Gupta, O. Aftenieva, P. T. Probst, S. Sarkar, A. M. Steiner, N. Vogel, A. Fery, T. A. F. König, *Adv. Photonics Res.* **2022**, *3*, 2200152.
[65] B. Nikoobakht, M. A. El-Sayed, *Chem. Mater.* **2003**, *15*, 1957.